SUPPORTING INFORMATION

I. COMPUTATIONAL DETAILS

Our calculations were performed by VASP (5.4.4) [1] using a plane wave basis set with the projector augmented wave (PAW) method [2]. The plane-wave energy cutoff was set to 400eV. Standard pseudopotentials are used for C,N,I,Pb,H, including 4,5,7,4,1 valence electrons, respectively. For better performance, we use an optimized version of VASP for Γ-point calculations. This is allowed since VBM and CBM of $MAPbI_3$ are located at the Γ-point and the unit cell dimensions are rather large.

We usually employ a GGA-PBE functional [3]. All structures were relaxed at PBE-level until the Hellman-Feynman forces were below 0.01eV/Å. For selected cases a single-point calculation (without structural relaxation) is done, by employing the HSE hybrid functional [4] with a mixing parameter of 0.43 and SOC. This follows the approach of Du [5]. Last but not least, we include van der Waals interactions by the correction scheme (DFT-D3) proposed in [6], in all calculations.

Regarding the CH_3NH_3 (MA) molecule orientation, our VAC terminated case in fig. 1 of the main text employs an apolar orientation, as introduced by Quarti et al. [7], where half of the C atoms pointing up and half down. This avoids the formation of an electric dipole moment. In the case of MAI termination, the inner layers are apolar too. Only the outermost MA molecules have "topC" orientation, which is shown in Quarti et al. [7] to be the most stable MAI terminated surface. Still, the structure is mirrored along the (horizontal) central Pb-I plane to further ensure a cancellation of dipole moments.

To furthermore quantify the influence of surface trap densities to the PLQY, we calculate a stack averaged PLQY, defined as

$$\mathrm{PLQY} = \frac{\int dx R_r(x)}{\int dx G(x)} \tag{1}$$

with bimolecular (radiative) recombination rate R_r, generation rate G and stack depth x. We then calculate the change in QFLS

$$\Delta\mathrm{QFLS} = -k_B T \ln\{\mathrm{PLQY}\} \tag{2}$$

These quantities can be obtained via drift-diffusion simulation. Latter solves the coupled continuity and Poisson-equation including drift and diffusion currents in case of semiconductors. The Transfer-matrix method is used for optical properties. Source or sink

terms are used within the continuity equation, to model trap-assisted and bimolecular recombination processes, as well as generation due to illumination. An overview of these processes is given in SI fig. 4. Values for different surface trap densities will be compared and perhaps explain the reduced PLQY in Warby et al. [8].

For drift-diffusion simulations, we use the commercial semiconductor-optics software SETFOS 5.4.13 [9]. Our stack consists of glass(1mm)/perovskite (500nm)/C_{60}(30nm)/ air(100nm), representing the experimental stack, used in Warby et al. [8]. All electronic parameters $\varepsilon_{\mathrm{HOMO}}, \varepsilon_{\mathrm{LUMO}}, N_{0,n}, N_{0,p}, \varepsilon_r, \mu_e, \mu_h$ for perovskite and C_{60} are adapted from Diekmann et al. [10], except for the mobility, which is chosen to be $10\mathrm{cm}^2/\mathrm{Vs}$ for electrons and holes. This is a lower estimate, since triple cation and or mixed halide perovskites have mobilities up to $35\mathrm{cm}^2/\mathrm{Vs}$ [11, 12]. For a table, see SI table V. Perovskite surface and bulk trap parameters can be found in SI, table IV to V and are adapted from [13, 14]. For C_{60} we use the Langevin recombination, described in SI. The stack is illuminated from the left side, using 500nm monochromatic light (1nm spectral width) and an intensity of $589.2\mathrm{W}/\mathrm{m}^2$. This intensity yields the same photon current as the sun, if only photons above the bandgap (1.68eV) are absorbed.

Since, the surface traps are of major importance in our drift-diffusion simulations, we highlight their implementation in SETFOS. The coupled continuity and Poisson-equation including drift and diffusion currents in case of semiconductors are the basis of this simulation. Then, source and sink terms are used within the continuity equation, to model trap-assisted recombination processes. For an exemplary electron trap at the surface, this results in following differential equation

$$\begin{aligned}\frac{\partial n_t^{\mathrm{Int}}}{\partial t} = &\left(N_t^{\mathrm{Int}} - n_t^{\mathrm{Int}}\right)\left(C_n^{e,l} n^l + C_n^{e,r} n^r + E_p^{e,l} + E_p^{e,r}\right) \\ &- n_t^{\mathrm{Int}}\left(C_p^{e,l} p^l + C_p^{e,r} p^r + E_n^{e,l} + E_n^{e,r}\right) \end{aligned} \tag{3}$$

where N_t^{int} is the electron trap density at the perovskite/C_{60} interface and n^l, p^l or n^r, p^r the left/right sided (free) carrier densities, respective to the interface. Latter quantities couple this rate equation to the general stack depth dependent continuity and Poisson-equation. Processes and corresponding capture coefficients are indicated in SI fig. 4. Upper rate equation allows carrier trapping due to perovskite surface traps, for carriers originating from perovskite and C_{60}.

II. COMMENT ON MIXING PARAMETER FOR HYBRID FUNCTIONALS

For the calculations with the HSE hybrid functional [4], the mixing parameter is set to 0.43. This is consistent with standard literature [14] for tetragonal $MAPbI_3$ bulk calculations, to yield the correct bandgap. For slab-models, it is consistent to keep this value, as done by [15]. This might result in apparently overestimated bandgaps for slab-models. Since the bulk bandgap was correct, this overestimation has physical reasons, as discussed in Haruyama et al. [16] who attributed this feature to PbI_6 distortions.

III. ADDITIONAL PARTIAL DENSITY OF STATES

We supply the partial density of states for the VAC:I_i, missing in the main text. Furthermore VAC:I_i and VAC:V_I are supplied for the HSE-level. The plots were created with less broadening and appear more sharp, to identify trap states close to the valence band.

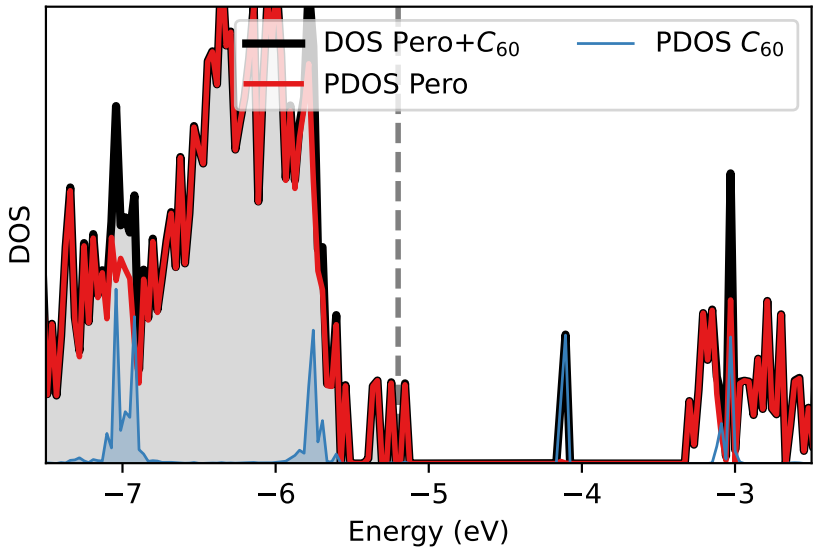

FIG. 1. Partial density of states at PBE-level for VAC:I_i showing trap states close to the valence band with contribution of perovskite only.

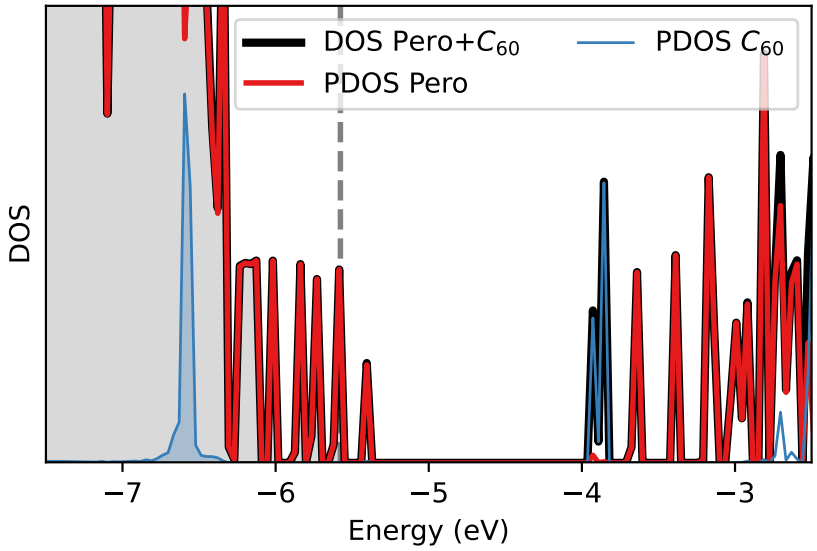

FIG. 2. Partial density of states at HSE-level for VAC:I_i showing trap states close to the valence band with contribution of perovskite only.

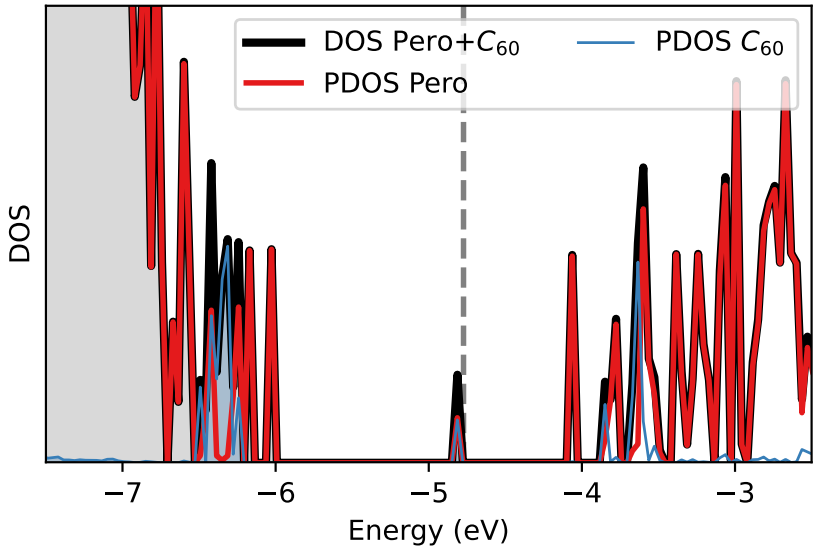

FIG. 3. Partial density of states at HSE-level for VAC:V_I showing midgap states with joint contribution of perovskite and C_{60}.

IV. C_{60} ADSORPTION ENERGIES AND DSE'S

A. At PBE-level

TABLE I. Adsorption energies (in eV) of C_{60} at PBE-level for different surface terminations and the contribution from dispersion (DFT-D3). Furthermore, we show adsorption energies in case of defective surfaces and their DSE. For the positions of defect and C_{60}, see fig. 2 in main text and SI VI.

System	E_{ads}	$E_{\text{ads}}^{\text{disp}}$	DSE	DSE^{disp}
MAI+C_{60} (above bridge)	-0.48	-0.49		
VAC+C_{60} (above Pb)	-0.53	-0.45		
MAI:Pb_i+C_{60}	-1.14	-0.67	0.67	0.18
VAC:I_i+C_{60}	-0.53	-0.60	0.04	0.15
VAC:V_I+C_{60}	-1.19	-0.52	0.66	0.07

B. At HSE-level

TABLE II. Adsorption energies (in eV) of C_{60} at HSE-level for VAC termination and the contribution from dispersion (DFT-D3). Furthermore, we show adsorption energies in case of defective surfaces and their respective DSE. The structure is equivalent to the PBE case. The MAI:Pb_i+C_{60} case was left out due to high computational costs.

System	E_{ads}	$E_{\text{ads}}^{\text{disp}}$	DSE	DSE^{disp}
VAC+C_{60} (above Pb)	-0.58	-0.45		
VAC:I_i+C_{60}	-0.45	-0.60	-0.14	0.15
VAC:V_I+C_{60}	-0.74	-0.52	0.16	0.07

C. Additional Theory

1. Adsorption Energy

The adsorption energy is defined as

$$E_{\text{ads}} = E_{\text{tot}}[\text{complex}] - E_{\text{tot}}[\text{adsorbent}] - E_{\text{tot}}[\text{adsorbate}] \tag{4}$$

Alternatively, we can use the dispersion (DFT-D3) contribution E_{disp}, instead of the total energy E_{tot}.

$$E_{\text{ads,disp}} = E_{\text{disp}}[\text{complex}] - E_{\text{disp}}[\text{adsorbent}] - E_{\text{disp}}[\text{adsorbate}] \tag{5}$$

2. Defect Formation Energy

The defect formation energy (DFE) of an uncharged point defect X, is given by [17]

$$\text{DFE}[X] = E_{\text{tot}}[\text{P+X}] - E_{\text{tot}}[\text{P}] - \sum_i n_i \mu_i \tag{6}$$

where $E_{\text{tot}}[\text{P+X}]$ is the total energy of our supercell, containing $MAPbI_3$, optionally C_{60} and the defect. $E_{\text{tot}}[\text{P}]$ is the total energy of our pristine supercell without a defect. Furthermore n_i is the number of added (removed) species i, to create the defect X, with respective chemical potentials μ_i. We will not use this notion, except for the derivation in the next section.

3. About Defect Stabilization Energies

Here we show, that the difference of DFE's, with or without C_{60} is equivalent to the difference of adsorption energies of C_{60} with or without presence of defects. Those differences define the defect stabilization energy (DSE) in eq. 2.

Let DFE$'$ denote the defect formation energy with presence of C_{60}, DFE without. Furthermore, $E_{\text{tot}}[\text{P+C+X}]$ denotes the total energy of the defective supercell, with $MAPbI_3$

and C_{60}, while E_{tot}[P+X] excludes the latter.

$$\mathrm{DFE'} - \mathrm{DFE} = E_{\mathrm{tot}}[\mathrm{P{+}C{+}X}] - E_{\mathrm{tot}}[\mathrm{P{+}C}] - \sum_i n_i \mu_i \tag{7}$$

$$- E_{\mathrm{tot}}[\mathrm{P{+}X}] + E_{\mathrm{tot}}[\mathrm{P}] + \sum_i n_i \mu_i \tag{8}$$

$$\begin{aligned} &= (E_{\mathrm{tot}}[\mathrm{P{+}C{+}X}] - E_{\mathrm{tot}}[\mathrm{P{+}X}] - E_{\mathrm{tot}}[\mathrm{C}]) \\ &\qquad - (E_{\mathrm{tot}}[\mathrm{P{+}C}] - E_{\mathrm{tot}}[\mathrm{P}] - E_{\mathrm{tot}}[\mathrm{C}]) \end{aligned} \tag{9}$$

$$= E_{\mathrm{ads}}^{\mathrm{def.}} - E_{\mathrm{ads}}^{\mathrm{prist.}} \tag{10}$$

4. Charge Density Differences

We calculate the charge density differences of valence electrons in fig. 1 given by

$$\Delta\rho = \rho_{\mathrm{MAPbI_3{+}C_{60}}} - \rho_{\mathrm{MAPbI_3}} - \rho_{\mathrm{C_{60}}} \tag{11}$$

The structure of the separated systems are fixed, relative to the combined one. Ionic contributions to charges will cancel each other. Thus, a positive value corresponds to electron-enriched regions caused by redistribution of charges, when the separated systems are combined. Vice versa negative values are depleted regions. A possible mechanism for observed charge redistribution could be different occupation numbers in the combined system. For example a before occupied defect orbital could be now unoccupied, by occupying the LUMO instead. This can be described by an offset of Fermi levels (of perovskite and C_{60}), which will align after perovskite and C_{60} have been brought into contact. Similar, a redistribution of charges can occur for $T > 0$K, where the occupation-statistic of orbitals are smeared.

Instead, we argue that the redistribution is mainly attributed to hybridization, since we found hybrid orbitals with equally distributed defect or C_{60} LUMO character.

V. DRIFT-DIFFUSION STANDARD PARAMETERS

For C_{60} we use the Langevin recombination

$$R_L = \gamma np = \eta \frac{e}{\varepsilon_0 \varepsilon_r} (\mu_e + \mu_h) np \tag{12}$$

where η is the recombination efficiency based on the morphology of a solar cell device. Since we have a planar structure $\eta = 1$ is a reasonable assumption.

TABLE III. List of used electronic parameters, adapted from [10], except for hole mobility of perovskite.

Parameter	Value
Relative permittivity C_{60}	5.0
Relative permittivity perovskite	22
Effective electron density C_{60}	$1 \times 10^{20}\text{cm}^{-3}$
Effective electron density perovskite	$2.2 \times 10^{18}\text{cm}^{-3}$
Electron mobility C_{60}	$0.001\text{cm}^2/\text{Vs}$
Electron mobility perovskite	$10\text{cm}^2/\text{Vs}$
Hole mobility C_{60}	$1 \times 10^{-6}\text{cm}^2/\text{Vs}$
Hole mobility perovskite	$10\text{cm}^2/\text{Vs}$
Electron affinity C_{60}	3.9eV
Electron affinity perovskite	3.9eV
Bandgap C_{60}	2.0eV
Bandgap perovskite	1.63eV

TABLE IV. List of used perovskite bulk trap parameters. Trap densities are adapted from [14] and trap rates and depths from [13].

Parameter	Electron/Acceptor traps	Hole/Donor traps
Trap density N_t (cm^{-3})	9×10^{13}	9×10^{13}
Trap energy depth E_t (eV)	0.85 (CB)	1.15 (VB)
Electron capture rate C_n^e,C_n^h (cm^3s^{-1})	1×10^{-7}	5×10^{-9}
Hole capture rate C_p^e,C_p^h (cm^3s^{-1})	3.5×10^{-8}	1×10^{-5}

TABLE V. List of used surface trap parameters.

Parameter	Value
Trap energy level E_t (eV)	4.8
Electron capture rate left $C_n^{h,l}(\text{cm}^3\text{s}^{-1})$	1×10^{-8}
Electron capture rate right $C_n^{h,r}(\text{cm}^3\text{s}^{-1})$	1×10^{-8}
Hole capture rate left $C_p^{h,l}(\text{cm}^3\text{s}^{-1})$	1×10^{-7}
Hole capture rate right $C_p^{h,r}(\text{cm}^3\text{s}^{-1})$	1×10^{-12}

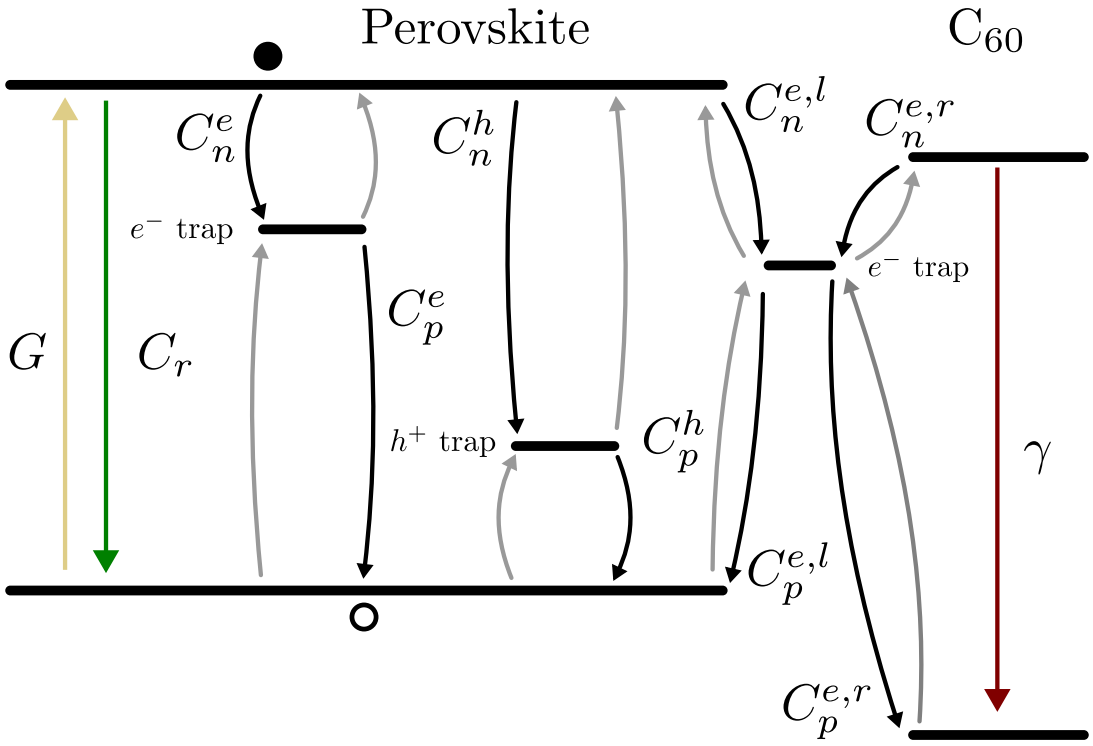

FIG. 4. Several processes for generation and recombination are shown. Recombinations are labeled with their corresponding capture coefficient. All arrows indicate the transition of electrons. The reverse emission process is indicated in grey.

VI. GEOMETRIES AND WAVEFUNCTIONS

We show all used geometries combined with all relevant wavefunctions. Latter are shown as their projected contribution to the charge density (also if not occupied). This is done, by plotting the PARCHG-files. For atomic labels please see fig. 6.1. Because of the hybridization, when introducing C_{60} or defects (or both), we need to redefine the notions of VBM, CBM and LUMO. This is done by indicating the new quantity with a prime. Shown orbitals in fig. 4 correspond to 571 (UP) and 690 (UP) for MAI:Pb_i (without/with C_{60}), 644 (DW) and 764 (DW) for VAC:I_i as well as 637 (UP) and 757 (UP) for VAC:V_I.

Color-Code:

Defects LUMO

VBM CBM

(Only lowest LUMO's are labeled)

PBE-level

Defects - without C60

MAI_Pbi

#	Energy(eV)	UP	DW	Occup. UP	DW	
569	-2.321014	-2.320632	1.000000	1.000000	VBM'	
570	-0.681761	-0.362963	1.000000	0.000000	DEF1'	
571	-0.644944	-0.345358	1.000000	0.000000	DEF2'	
572	-0.364168	-0.338410	0.000000	0.000000	CBM'	

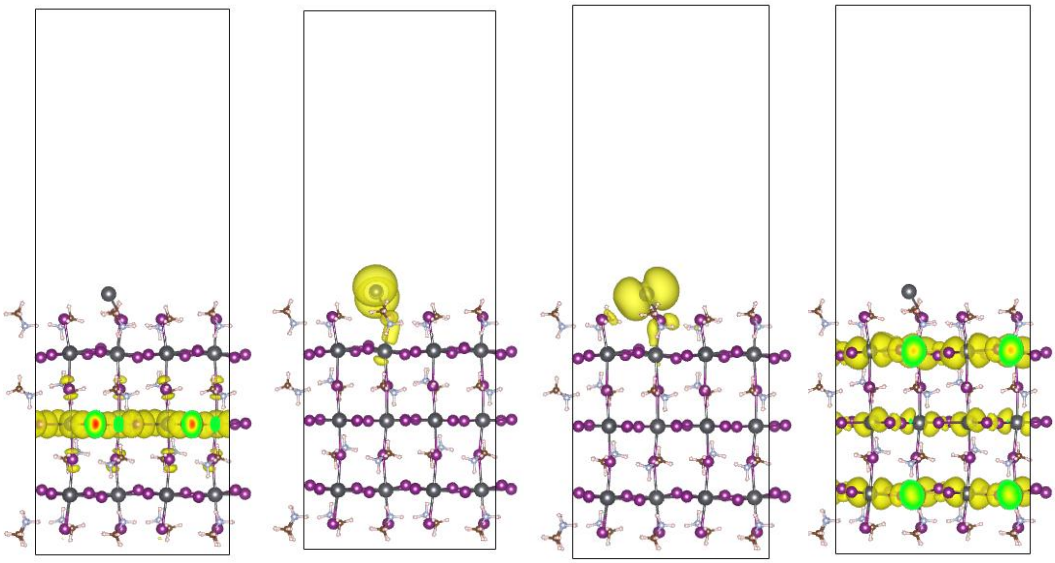

569 (UP+DW) 570 UP 571 UP 572 UP

VAC_Ii

642	-2.126262	-2.125312	1.000000	1.000000	VBM'
643	-2.087190	-2.012737	1.000000	1.000000	
644	-2.008094	-1.871249	1.000000	0.000000	DEF'
645	-0.097964	-0.097316	0.000000	0.000000	CBM'

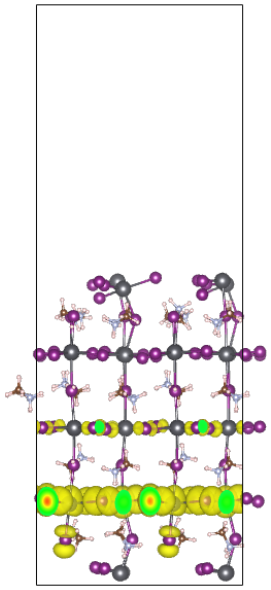

642(UP+DW)

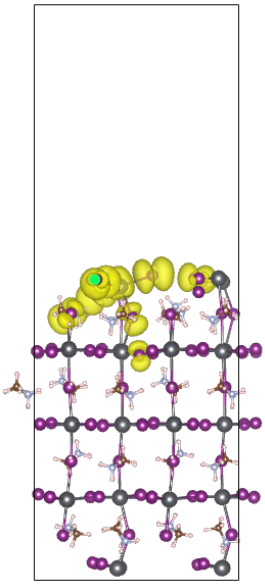

643 UP

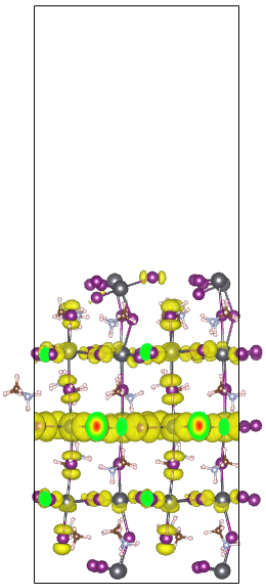

643 DW

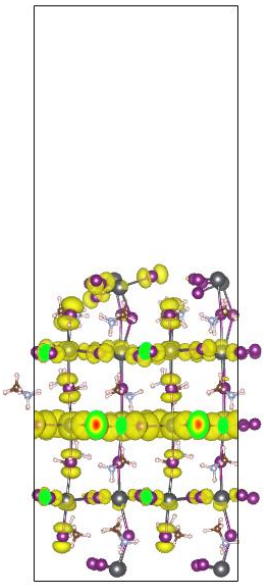

644 UP

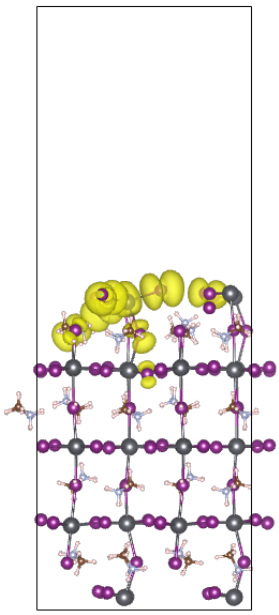

644 DW

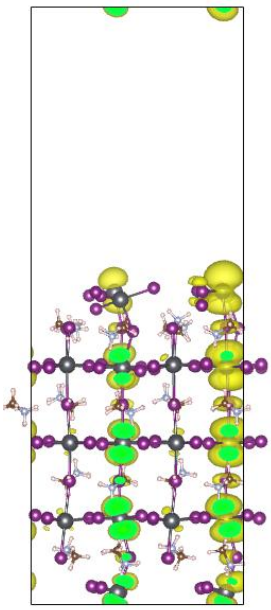

645 (UP+DW)

VAC_VI

636	-2.019797	-2.019544	1.000000 1.000000	VBM’
637	-0.745388	-0.115380	1.000000 0.000000	DEF’
638	-0.113652	-0.045238	0.000000 0.000000	CBM’

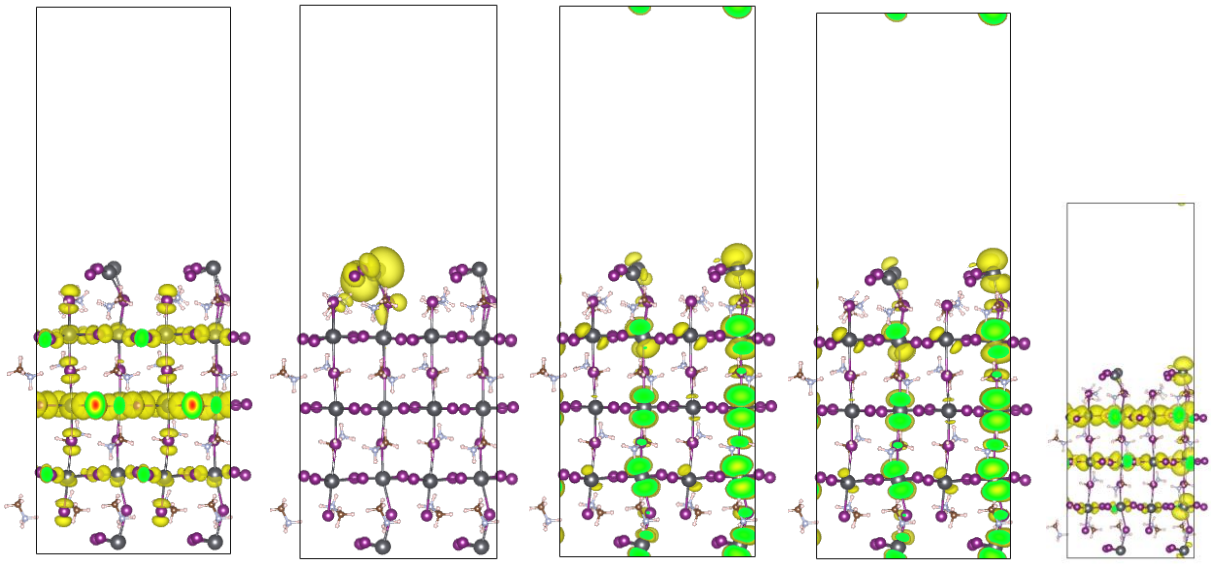

636 (UP+DW) 637 UP 637 DW 638 UP 638 DW

Defects - with C60

MAI_Pbi

689	-2.092766	-2.092633	1.000000	1.000000	VBM’
690	-1.476877	-1.144346	1.000000	0.000000	
691	-1.199384	-0.918117	1.000000	0.000000	DEF’
692	-0.928726	-0.901347	0.000000	0.000000	LUMO’
693	-0.878759	-0.329730	0.000000	0.000000	
694	-0.692720	-0.145975	0.000000	0.000000	
695	-0.133137	-0.130918	0.000000	0.000000	CBM’
696	-0.112673	-0.112333	0.000000	0.000000	

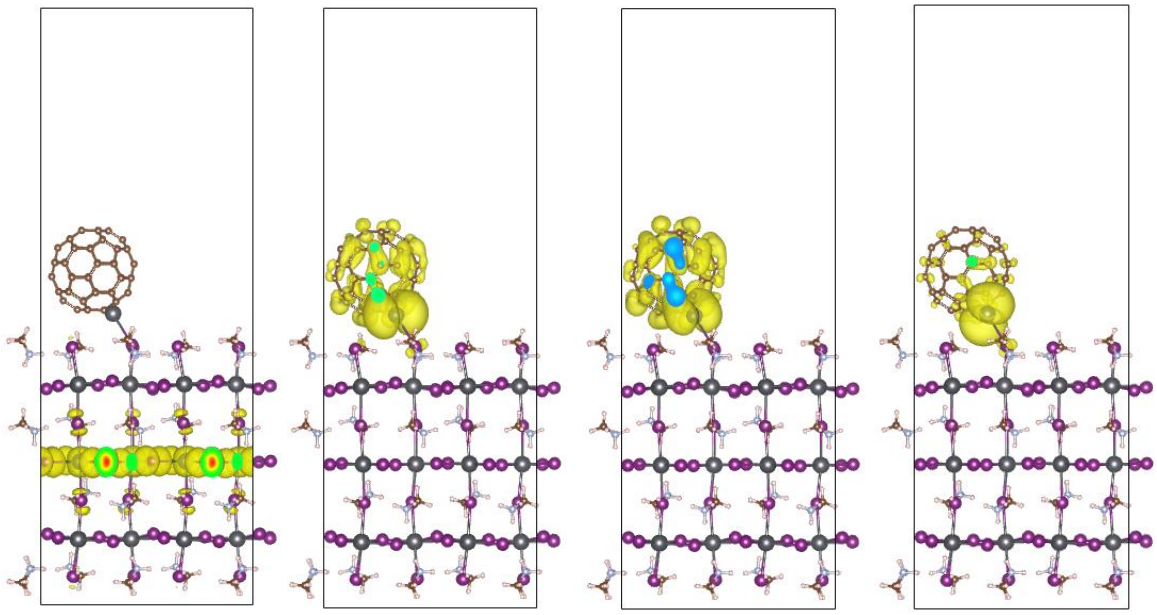

689 (UP+DW) 690 UP 690 DW 691 UP

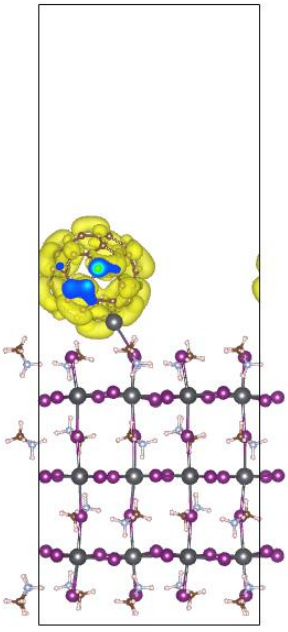

691 DW

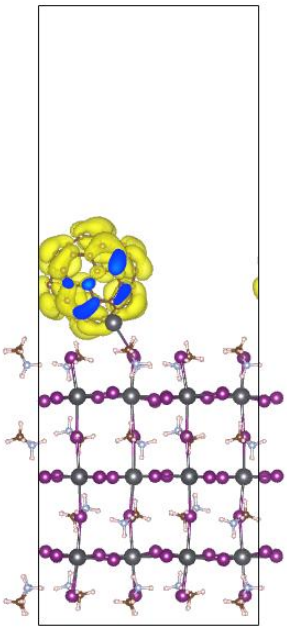

692 UP

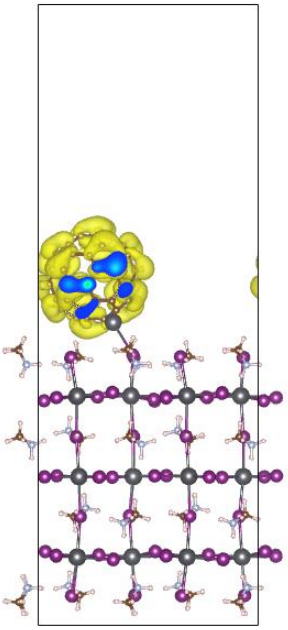

692 DW

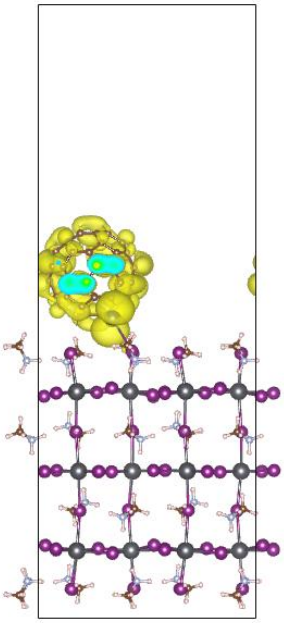

693 UP

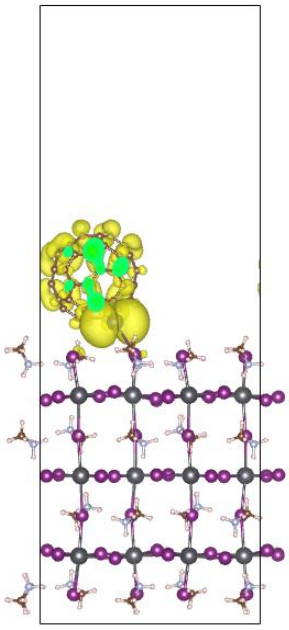

693 DW

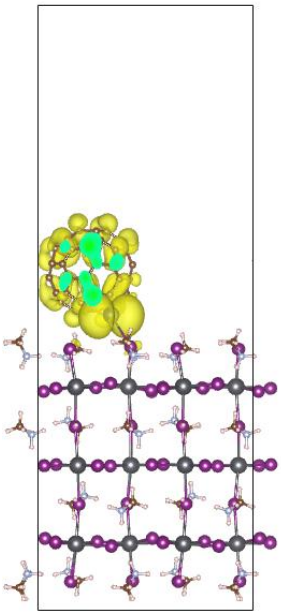

694 UP

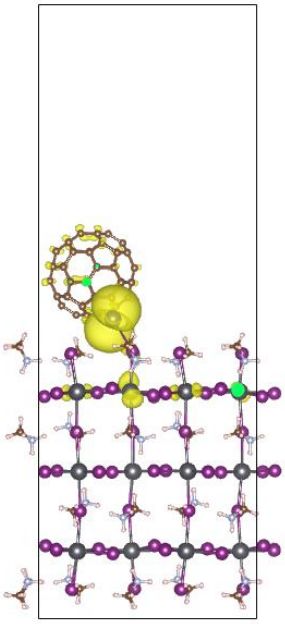

694 DW

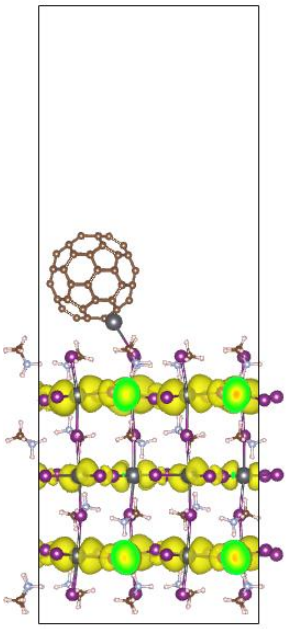

694 UP

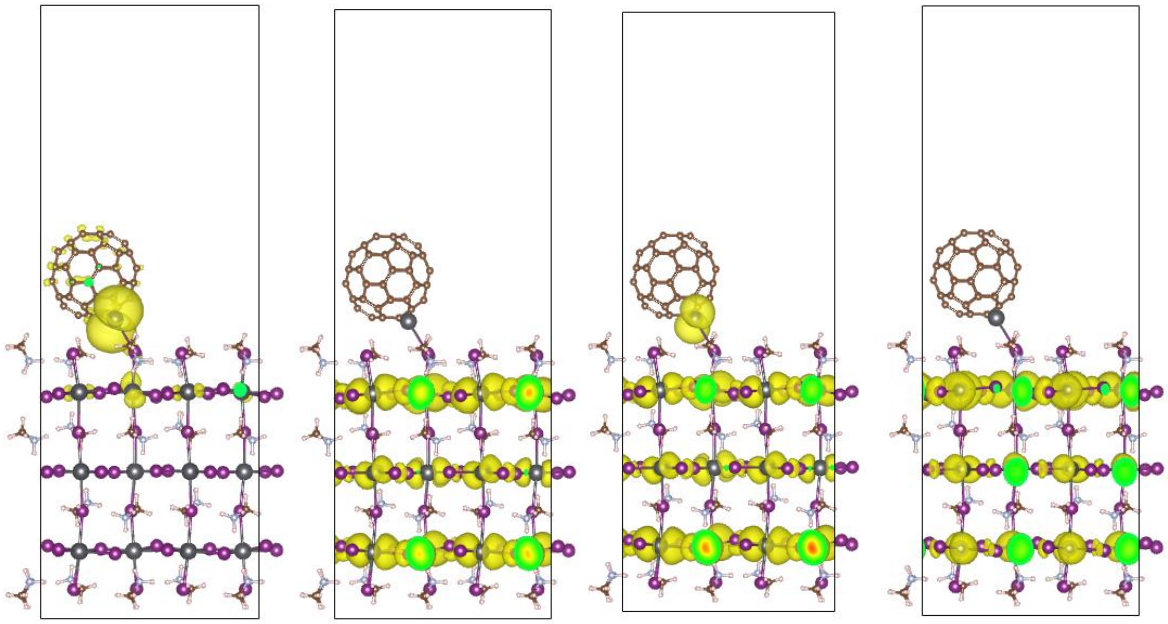

694 DW 695 UP 695 DW 696 (UP+DW)

VAC_li

761	-1.874249	-1.851123	1.000000	1.000000	
762	-1.823187	-1.812728	1.000000	1.000000	
763	-1.797303	-1.715143	1.000000	1.000000	VBM’
764	-1.691399	-1.637526	1.000000	0.000000	DEF’
765	-0.622264	-0.619507	0.000000	0.000000	LUMO’
766	-0.589569	-0.588527	0.000000	0.000000	
767	-0.585400	-0.584362	0.000000	0.000000	
768	0.235833	0.237097	0.000000	0.000000	CBM’
769	0.293895	0.294829	0.000000	0.000000	
770	0.310280	0.311123	0.000000	0.000000	

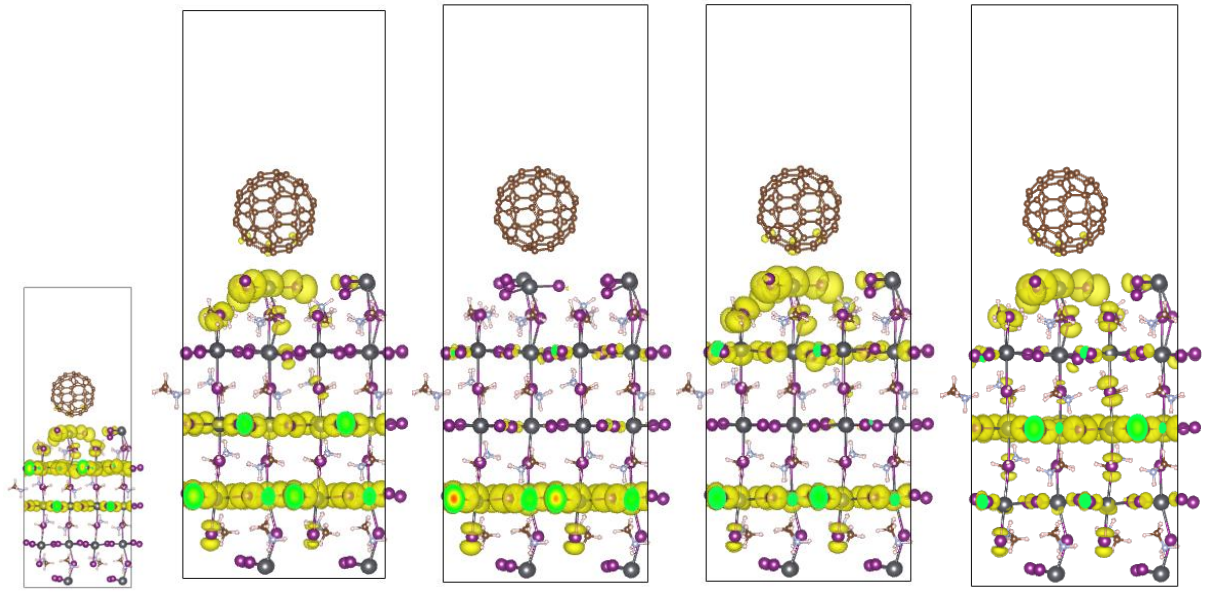

761 (UP+DW) 762 UP 762 DW 763 UP 763 DW

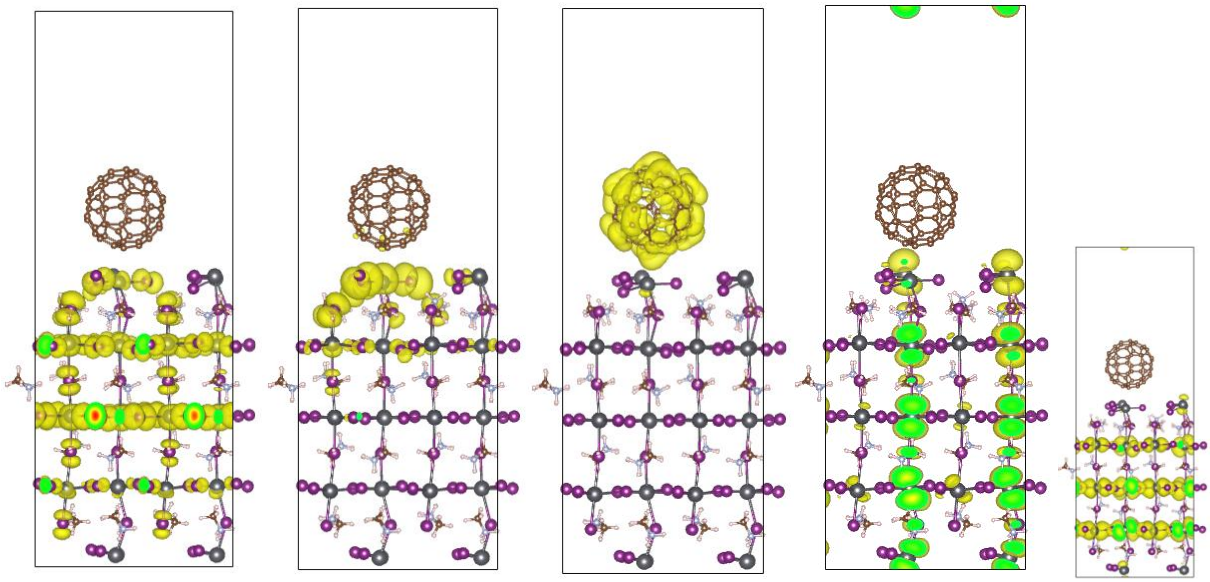

764 UP | 764 DW | 765 (UP+DW) | 768 (UP+DW) | 769 (U+D)

VAC_VI

755	-1.850031	-1.831802	1.000000	1.000000	
756	-1.841934	-1.815993	1.000000	1.000000	VBM’
757	-0.681708	-0.479968	1.000000	0.000000	DEF’
758	-0.240526	-0.220987	0.000000	0.000000	LUMO’
759	-0.222189	-0.202245	0.000000	0.000000	
760	-0.005263	0.068397	0.000000	0.000000	CBM’
761	0.095528	0.144466	0.000000	0.000000	
762	0.144048	0.152082	0.000000	0.000000	
763	0.164173	0.164608	0.000000	0.000000	

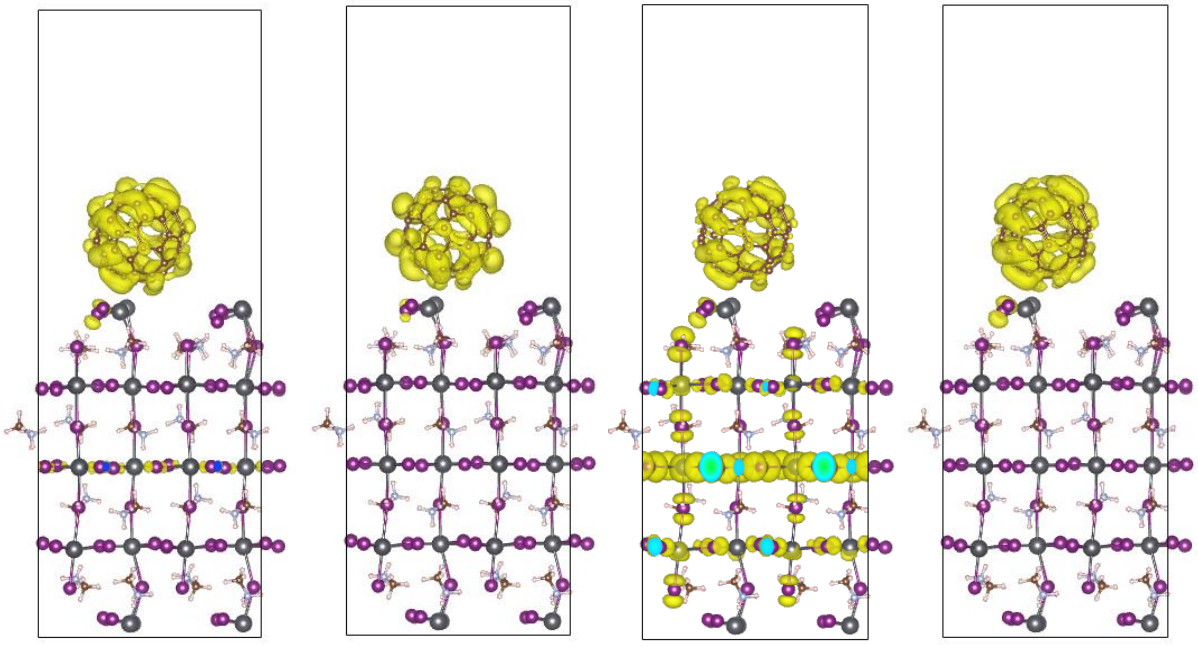

755 UP | 755 DW | 756 UP | 756 DW

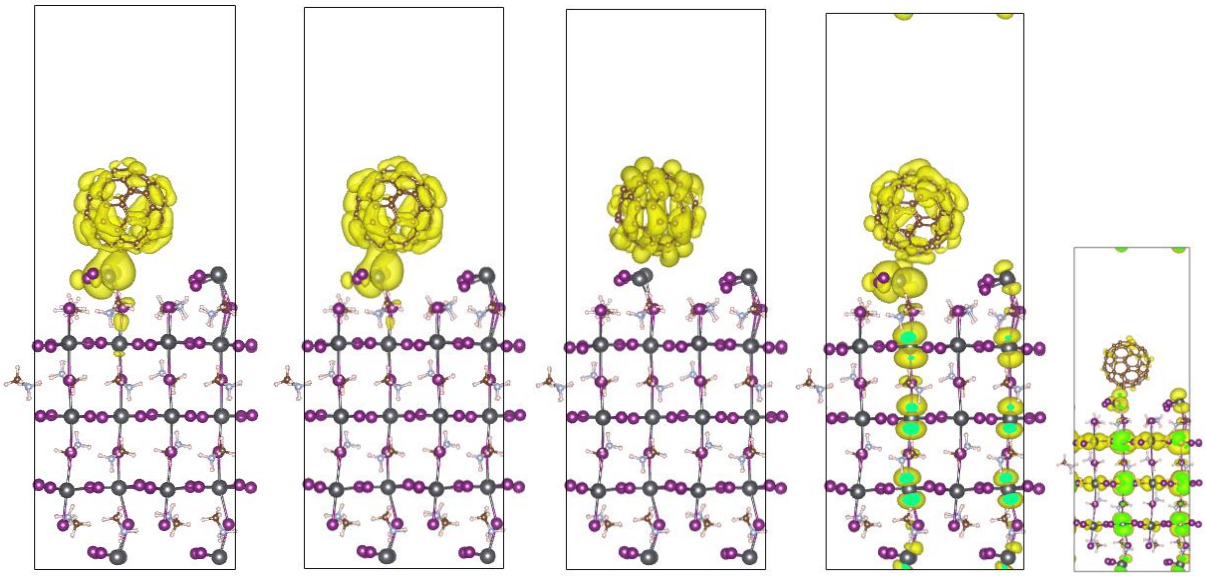

757 UP 757 DW 758 (UP+DW) 760 (UP+DW) 761 (U+D)

HSE+SOC-level

Defects - without C60

VAC_Ii

1287	-2.609510	1.000000	VBM’
1288	-1.919479	0.000000	DEF’
1289	-0.655507	0.000000	CBM’

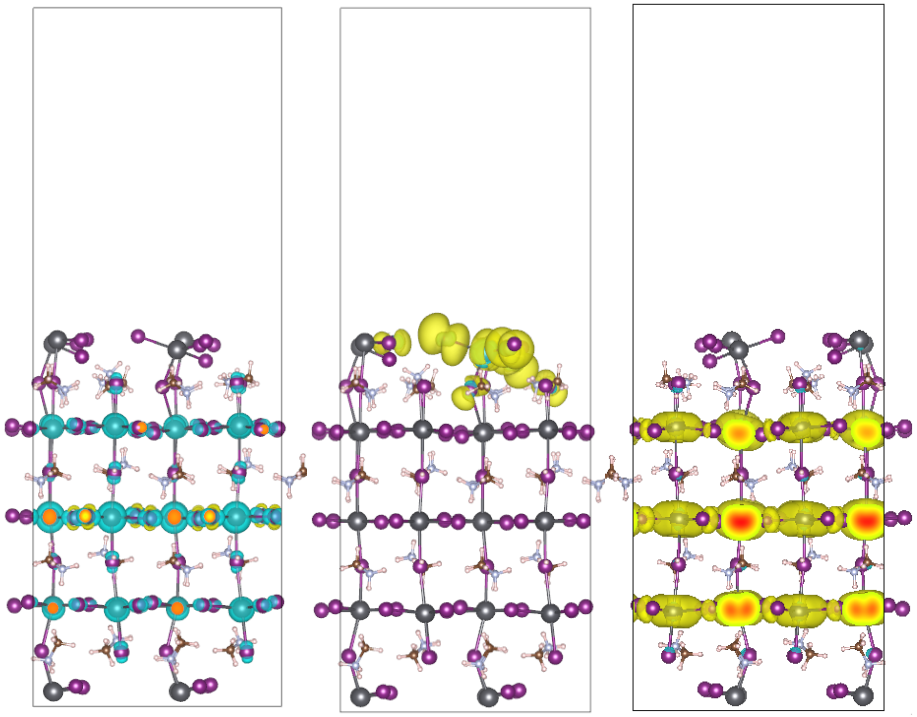

1287 1288 1289

VAC_VI

1272	-2.638356	1.000000	VBM’
1273	-1.789830	1.000000	DEF’
1274	-0.699830	0.000000	CBM’

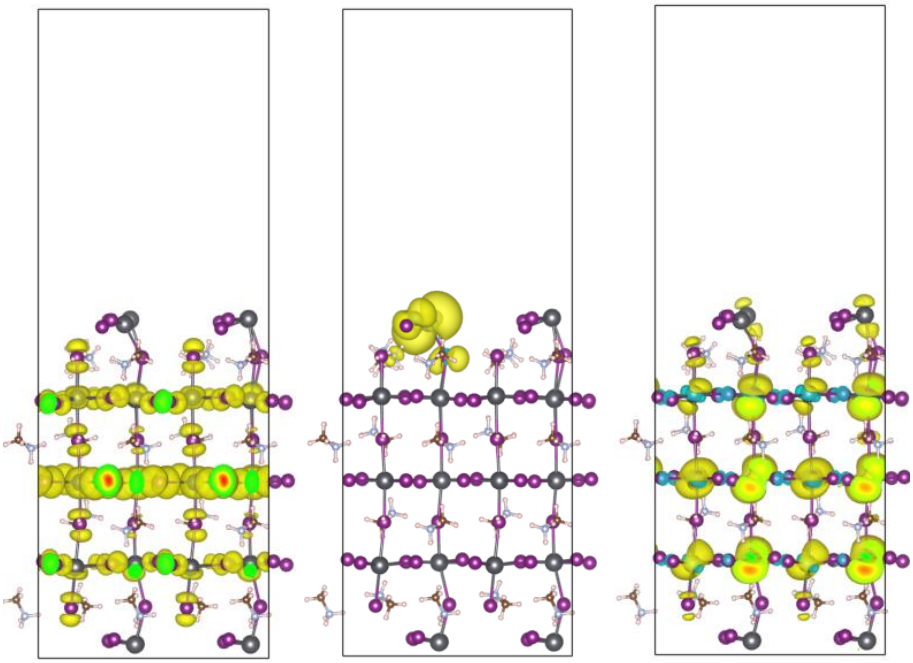

1272 1273 1274

Defects - with C60

VAC_Ii

1527	-2.203475	1.000000	VBM’
1528	-2.008354	0.000000	DEF’
1529	-0.533457	0.000000	LUMO’
1530	-0.523892	0.000000	
1531	-0.477302	0.000000	
1532	-0.474996	0.000000	
1533	-0.469050	0.000000	
1534	-0.466673	0.000000	
1535	-0.259320	0.000000	CBM’

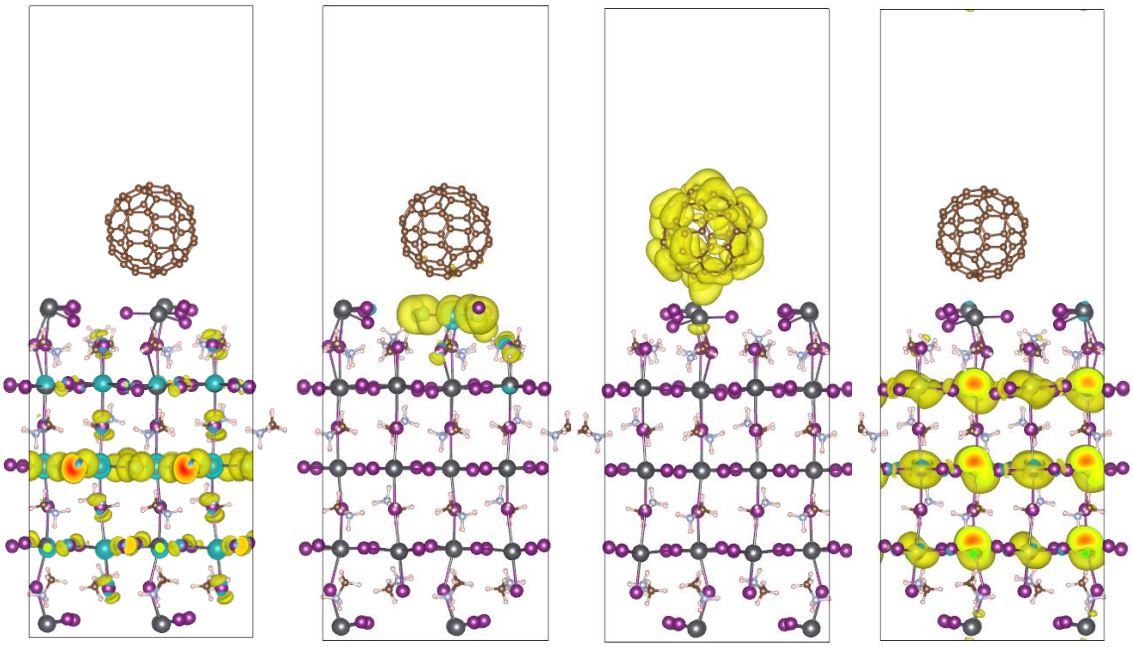

1527 1528 1529 1535

VAC_VI

1512	-2.418263	1.000000	VBM’
1513	-1.202088	1.000000	DEF’
1514	-0.466128	0.000000	CBM’

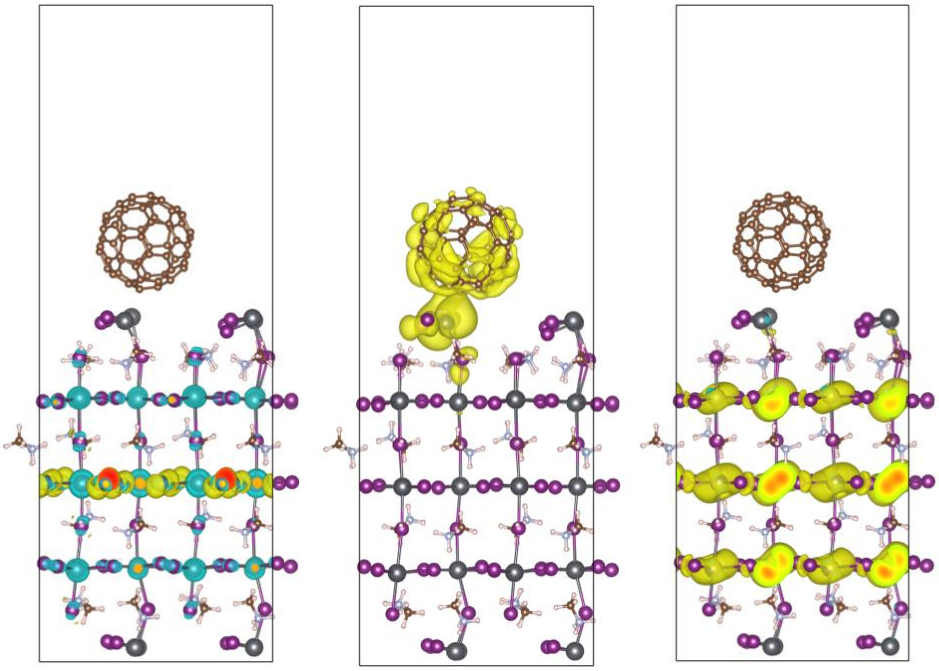

1512 1513 1514

[1] G. Kresse and J. Furthmüller, Phys. Rev. B **54**, 11169 (1996).

[2] P. E. Blöchl, Phys. Rev. B **50**, 17953 (1994).

[3] J. P. Perdew, K. Burke, and M. Ernzerhof, Phys. Rev. Lett. **77**, 3865 (1996).

[4] J. Heyd, G. E. Scuseria, and M. Ernzerhof, The Journal of Chemical Physics **124**, 219906 (2006), https://pubs.aip.org/aip/jcp/article-pdf/doi/10.1063/1.2204597/15387022/219906_1_online.pdf.

[5] M.-H. Du, The Journal of Physical Chemistry Letters **6**, 1461 (2015), pMID: 26263152, https://doi.org/10.1021/acs.jpclett.5b00199.

[6] S. Grimme, J. Antony, S. Ehrlich, and H. Krieg, The Journal of Chemical Physics **132**, 154104 (2010), https://pubs.aip.org/aip/jcp/article-pdf/doi/10.1063/1.3382344/15684000/154104_1_online.pdf.

[7] C. Quarti, F. De Angelis, and D. Beljonne, Chemistry of Materials **29**, 958 (2017), https://doi.org/10.1021/acs.chemmater.6b03259.

[8] J. Warby, F. Zu, S. Zeiske, E. Gutierrez-Partida, L. Frohloff, S. Kahmann, K. Frohna, E. Mosconi, E. Radicchi, F. Lang, S. Shah, F. Peña-Camargo, H. Hempel, T. Unold, N. Koch, A. Armin, F. De Angelis, S. D. Stranks, D. Neher, and M. Stolterfoht, Advanced Energy Materials **12**, 2103567 (2022), https://onlinelibrary.wiley.com/doi/pdf/10.1002/aenm.202103567.

[9] U. Aeberhard, S. Altazin, L. Stepanova, A. Stous, B. Blülle, C. Kirsch, E. Knapp, and B. Ruhstaller, in *2019 IEEE 46th Photovoltaic Specialists Conference (PVSC)* (2019) pp. 0105–0111.

[10] J. Diekmann, P. Caprioglio, M. H. Futscher, V. M. Le Corre, S. Reichert, F. Jaiser, M. Arvind, L. P. Toro, E. Gutierrez-Partida, F. Peña-Camargo, C. Deibel, B. Ehrler, T. Unold, T. Kirchartz, D. Neher, and M. Stolterfoht, Solar RRL **5**, 2100219 (2021), https://onlinelibrary.wiley.com/doi/pdf/10.1002/solr.202100219.

[11] A. Al-Ashouri, E. Köhnen, B. Li, A. Magomedov, H. Hempel, P. Caprioglio, J. A. Márquez, A. B. M. Vilches, E. Kasparavicius, J. A. Smith, N. Phung, D. Menzel, M. Grischek, L. Kegelmann, D. Skroblin, C. Gollwitzer, T. Malinauskas, M. Jošt, G. Matič, B. Rech, R. Schlatmann, M. Topič, L. Korte, A. Abate, B. Stannowski, D. Neher, M. Stolterfoht, T. Unold, V. Getautis, and S. Albrecht, Science **370**, 1300 (2020),

https://www.science.org/doi/pdf/10.1126/science.abd4016.

[12] L. M. Herz, ACS Energy Letters **2**, 1539 (2017), https://doi.org/10.1021/acsenergylett.7b00276.

[13] X. Zhang, M. E. Turiansky, J.-X. Shen, and C. G. Van de Walle, Phys. Rev. B **101**, 140101 (2020).

[14] D. Meggiolaro, S. G. Motti, E. Mosconi, A. J. Barker, J. Ball, C. Andrea Riccardo Perini, F. Deschler, A. Petrozza, and F. De Angelis, Energy Environ. Sci. **11**, 702 (2018).

[15] H. Uratani and K. Yamashita, The Journal of Physical Chemistry Letters **8**, 742 (2017), pMID: 28129504, https://doi.org/10.1021/acs.jpclett.7b00055.

[16] J. Haruyama, K. Sodeyama, L. Han, and Y. Tateyama, The Journal of Physical Chemistry Letters **5**, 2903 (2014), pMID: 26278097, https://doi.org/10.1021/jz501510v.

[17] C. Freysoldt, B. Grabowski, T. Hickel, J. Neugebauer, G. Kresse, A. Janotti, and C. G. Van de Walle, Rev. Mod. Phys. **86**, 253 (2014).